Calcium supplementation of bioinks reduces shear stress-induced cell damage during bioprinting

Biofabrication

PAPER

Calcium supplementation of bioinks reduces shear stress-induced cell damage during bioprinting

Lena Fischer[1], Mojtaba Nosratlo[1], Katharina Hast[1], Emine Karakaya[2], Nadine Ströhlein[1], Tilman U Esser[3], Richard Gerum[1,4], Sebastian Richter[1], Felix Engel[3], Rainer Detsch[2], Ben Fabry[1] and Ingo Thievessen[1,*]

[1] Department of Physics, University of Erlangen-Nuremberg, Erlangen, Germany
[2] Institute of Biomaterials, Department of Materials Science and Engineering, University of Erlangen-Nuremberg, Erlangen, Germany
[3] Experimental Renal and Cardiovascular Research, Department of Nephropathology, Institute of Pathology, Friedrich-Alexander-University of Erlangen-Nuremberg, Erlangen, Germany
[4] Department of Physics and Astronomy, York-University Toronto, Ontario, Canada
* Author to whom any correspondence should be addressed.

E-mail: ingo.thievessen@fau.de

Keywords: bioprinting, shear stress, cell viability, plasma membrane resealing, calcium, alginate, styryl dye

Supplementary material for this article is available online

OPEN ACCESS

RECEIVED
2 February 2022

REVISED
3 June 2022

ACCEPTED FOR PUBLICATION
27 July 2022

PUBLISHED
11 August 2022

Abstract

During bioprinting, cells are suspended in a viscous bioink and extruded under pressure through small diameter printing needles. The combination of high pressure and small needle diameter exposes cells to considerable shear stress, which can lead to cell damage and death. Approaches to monitor and control shear stress-induced cell damage are currently not well established. To visualize the effects of printing-induced shear stress on plasma membrane integrity, we add FM 1-43 to the bioink, a styryl dye that becomes fluorescent when bound to lipid membranes, such as the cellular plasma membrane. Upon plasma membrane disruption, the dye enters the cell and also stains intracellular membranes. Extrusion of alginate-suspended NIH/3T3 cells through a 200 μm printing needle led to an increased FM 1-43 incorporation at high pressure, demonstrating that typical shear stresses during bioprinting can transiently damage the plasma membrane. Cell imaging in a microfluidic channel confirmed that FM 1-43 incorporation is caused by cell strain. Notably, high printing pressure also impaired cell survival in bioprinting experiments. Using cell types of different stiffnesses, we find that shear stress-induced cell strain, FM 1-43 incorporation and cell death were reduced in stiffer compared to softer cell types and demonstrate that cell damage and death correlate with shear stress-induced cell deformation. Importantly, supplementation of the suspension medium with physiological concentrations of $CaCl_2$ greatly reduced shear stress-induced cell damage and death but not cell deformation. As the sudden influx of calcium ions is known to induce rapid cellular vesicle exocytosis and subsequent actin polymerization in the cell cortex, we hypothesize that calcium supplementation facilitates the rapid resealing of plasma membrane damage sites. We recommend that bioinks should be routinely supplemented with physiological concentrations of calcium ions to reduce shear stress-induced cell damage and death during extrusion bioprinting.

1. Introduction

Bioprinting enables the fabrication of tissue-like constructs with high resolution while maintaining cost efficiency and scalability [1]. Common bioprinting techniques include inkjet printing [2], laser-assisted printing [3] and extrusion printing [4]. Extrusion printing is currently the most popular method due to its affordability, the availability of bioinks with a wide range of viscosities, and the possibility to print at high cell densities [5, 6]. However, one major problem is the inevitable exposition of cells to fluid shear stress and extensional or compressive fluid stresses during the dispensing process.

In this study, we focus on fluid shear stress. The fluid shear stress inside a printing needle depends

on only two factors—printing pressure and printing needle geometry [7]. For a printing needle with cylindrical cross section, the fluid shear stress increases linearly with increasing radial position, from zero at the needle centre to a maximum value at the needle wall [7]. For a given radial position, the shear stress is constant along the length of the printing needle, if one ignores entrance and exit effects. The maximum shear stress at the needle wall increases linearly with higher printing pressure and larger inner diameter of the printing needle. Importantly, the fluid shear stress for a given printing pressure and needle geometry does not depend on the viscosity of the suspension fluid [7]. However, bioinks with a lower viscosity can be printed at a lower pressure, helping to limit maximum shear stresses. To counteract the low shape stability of low-viscosity bioinks, shear-thinning bioinks such as alginate [8–10] or hyaluronic acid [11–13] are widely used. However, for a typical 1 cm long printing needle with an inner diameter (ID) of 100 μm, the maximum fluid shear stress at the inner wall is 250 Pa at a pressure of 1 bar and increases to 1500 Pa at a pressure of 6 bar [7]. Such high shear stresses can induce noticeable cell damage. Indeed, previous studies reported that cell viability decreased considerably when the printing pressure was increased [14, 15].

Current thinking suggests that fluid shear stresses or extensional flow-mediated cell deformations can damage the plasma membrane and thus lead to reduced cell survival [15–17]. Hence, methods to directly detect effects of bioprinting on plasma membrane integrity would be useful for tuning printing parameters and improving cell-compatibility in bioprinting applications. However, methods that allow for a rapid and simple monitoring of plasma membrane integrity are currently lacking. Notably, strategies to limit the shear stress exposure of cells focus on modifications of the bioink, e.g. lowering the printing pressure by using shear thinning ink materials, or on optimizing the needle geometry [18, 19]. By contrast, approaches to directly reduce the cellular vulnerability to shear stress, e.g. by improving the resealing of the plasma membrane, or by increasing cell stiffness to reduce stress-induced cell deformations, have to the best of our knowledge previously not been implemented.

As an intracellular messenger, cytosolic calcium plays a fundamental role in cell signalling. Calcium regulates central processes such as gene expression or proliferation [20, 21]. Moreover, passive entry of calcium ions through leakages in the plasma membrane was shown to induce plasma membrane resealing and actin cytoskeleton remodelling [22, 23]. Even though cell shearing and plasma membrane damage are considered major causes of impaired cell survival or cell behaviour after bioprinting, a possible role of calcium in preventing the detrimental effects of membrane damage during bioprinting has thus far not been addressed, to our knowledge.

Using the lipid bilayer-incorporating fluorescent styryl dye FM 1-43, we developed an assay to monitor shear stress dependent damages to the plasma membrane during bioprinting. We demonstrate that the application of shear forces leads to an increased cellular uptake and fluorescence intensity of FM 1-43, indicating plasma membrane damage. Moreover, we report that bioprinting-induced shear stress does not impair cell proliferation but strongly impairs cell survival. Importantly, we show in cell types of different stiffnesses that cell damage and death correlate with shear stress-induced cell deformation. However, cell survival can be largely restored by supplementing the bioink with physiological concentrations of $CaCl_2$, presumably by calcium-driven exocytotic resealing of the plasma membrane or actin cortex remodelling. Taken together, our results demonstrate that calcium supplementation of the bioink protects cells against shear stress-induced damage during bioprinting.

2. Materials and methods

2.1. Cell cultivation

Parental NIH/3T3 mouse embryonic fibroblasts (ATCC, Wesel, Germany) as well as tdTomato-Farnesyl or FastFUCCI expressing NIH/3T3 cells were cultured in high-glucose (4.5 g l^{-1}) Dulbecco's modified Eagle's medium (Gibco™—Thermo Fisher Scientific, Massachusetts, USA), supplemented with 10% bovine calf serum (Sigma-Aldrich Chemie GmbH, Taufkirchen, Germany) and 1% penicillin/streptomycin (Gibco™—Thermo Fisher Scientific, Massachusetts, USA). A125 (ATCC, Wesel, Germany) and MDA-MB-231 (ATCC, Wesel, Germany) were cultured in high-glucose (4.5 g l^{-1}) Dulbecco's modified Eagle's medium (Gibco™—Thermo Fisher Scientific, Massachusetts, USA), supplemented with 10% fetal bovine serum (Sigma-Aldrich Chemie GmbH, Taufkirchen, Germany) and 1% penicillin/streptomycin (Gibco™—Thermo Fisher Scientific, Massachusetts, USA). HUVEC/Tert2 cells (ATCC, Wesel, Germany) were cultured in vascular cell basal medium (ATCC, Wesel, Germany) supplemented with endothelial growth kit-VEGF (ATCC, Wesel, Germany). Cells were passaged every second day using 0.25% trypsin/EDTA (Gibco™—Thermo Fisher Scientific, Massachusetts, USA). Human induced pluripotent stem cells (hiPSC, 'F1') [24] were cultured on Matrigel-coated culture plates or flasks in stem cell culture medium (StemMACS iPS-Brew XF, Miltenyi Biotec, Germany). Medium was exchanged daily. HiPSC were passaged every two to three days at 75%–80% confluency using EDTA (0.5 mM) and replated in stem cell culture medium supplemented with 10 μM rho-associated protein kinase (ROCK)-inhibitor

(Y-27632, Selleck Chemicals). For experimental usage, hiPSC were dissociated into single cell suspension using accutase (Sigma-Aldrich Chemie GmbH, Taufkirchen, Germany). All cells were cultured at 37 °C, 5% CO_2 and 95% humidity.

2.2. Generation of FastFUCCI and tdTomato-Farnesyl expressing NIH/3T3-based reporter cell lines

To monitor alterations in the plasma membrane conformation following shear stress application, we generated a NIH/3T3-based reporter cell line, stably expressing tdTomato fluorescent protein carrying a farnesylation-sequence, which targets tdTomato to the plasma membrane. For cell cycle analyses, we created a NIH/3T3-based cell line, stably expressing the fluorescent ubiquitination-based cell cycle indicator (FastFUCCI) reporter system. Using a 5′ primer encoding a *BamHI* site and a 3′ primer encoding a *NotI* site, the cDNA of the farnesylated tdTomato fluorescent protein was amplified from tdTomato-Farnesyl-5 (#58092, Addgene, Watertown, MA, USA) to replace the AcGFP cDNA in pLVX-AcGFP-N1 (#632154, Clontech Laboratories Inc.; Mountain View, CA, USA). The plasmid DNA was purified using the NucleoBond Xtra Maxi Kit (Macherey–Nagel, #740414.50) and its sequence was verified by custom DNA sequencing (Eurofins Genomics Germany GmbH, Ebersberg, Germany). NIH/3T3 cells stably expressing the tdTomato-Farnesyl or FastFUCCI reporter system were generated by lentiviral transduction. Lentivirus was produced by transfection of LentiX 293T cells (Takara Bio Europe SAS, Saint-Germain-en-Laye, France) with transfer plasmids pBOB-EF1-FastFUCCI-Puro (#86849, Addgene, Watertown, MA, USA) or pLVX-tdTomato-Farnesyl-N1, packaging plasmid psPAX2 (#2260, Addgene, Watertown, MA, USA) and envelope plasmid pCMV-VSV-G (#8454, Addgene, Watertown, MA, USA), using Lipofectamine 2000 reagent (Invitrogen—Thermo Fisher Scientific, Massachusetts, USA). Infectious lentivirus-containing supernatant was harvested 48 h post-transfection and centrifuged (500 g, 10 min). After ten-fold concentration, using the LentiX-concentrator (Takara Bio Europe SAS, Saint-Germain-en-Laye, France), the concentrated virus-containing medium was used to transduce NIH/3T3 cells, which were seeded 24 h in advance at a density of 100 000 per 9.6 cm^2. Successfully transduced NIH/3T3 cells were further selected with puromycin (5 $\mu g\ ml^{-1}$) (Gibco™—Thermo Fisher Scientific, Massachusetts, USA).

2.3. Synthesis of alginate-di-aldehyde (ADA)

Meta-periodate-based synthesis of ADA was performed as described previously [25]. Briefly, 50 ml of an aqueous 125 mM $NaIO_4$ (Sigma-Aldrich Chemie GmbH, Taufkirchen, Germany) solution were slowly added to 50 ml of 20% (w/v) alginate (Vivapharm alginate PH176, JRS Pharma GmbH, Rosenberg, Germany) dissolved in ethanol and stirred for 6 h. All reactions were carried out in the absence of light, to avoid side reactions of $NaIO_4$. The oxidation was stopped with 10 ml ethylene glycol (Sigma-Aldrich Chemie GmbH, Taufkirchen, Germany). The solution was left to rest for 10 min, the aqueous phase containing unwanted by-products was decanted, and the remaining ADA-phase was dissolved in 400 ml deionized water, prior to dialyzation (molecular weight cut-off (MWCO): 6000–8000 Da, Spectrum LAB, USA) in the absence of light for four days with daily water exchanges, and final lyophilization.

2.4. Hydrogel preparation

Sodium alginate (Vivapharm alginate PH176, JRS Pharma GmbH, Rosenberg, Germany) was dissolved in dulbecco′s phosphate buffered saline (DPBS); no calcium, no magnesium, Gibco™—Thermo Fisher Scientific, Massachusetts, USA) or DPBS supplemented with 1.9 mM $CaCl_2$ solution (calcium chloride dihydrate, Sigma-Aldrich Chemie GmbH, Taufkirchen, Germany) under constant stirring overnight to obtain a 2% (w/v) or 3% (w/v) hydrogel solution. For the generation of a 2.5% alginate di-aldehyde-gelatine (ADA-GEL) hydrogel, 5% of dry ADA and 5% of gelatine were dissolved in DPBS and ultrapure water, respectively. Afterwards, both solutions were mixed in a 1:1 volume ratio for 10 min at 37 °C, to obtain a 2.5% ADA-GEL solution, covalently crosslinked by Schiff's base formation. To prepare methacrylated gelatine (GelMA), 9% (w/v) lyophilized GelMA (Cellink, Gothenburg, Sweden) and 0.25% (w/v) of the photoinitiator lithium phenyl-2,4,6-trimethylbenzoylphosphinate (LAP; Cellink, Gothenburg, Sweden) were dissolved in DPBS or DPBS supplemented with 1.9 mM $CaCl_2$ at 40 °C. The reconstituted bioink was kept at 37 °C.

2.5. Bioprinting

For fluorescence-based detection of plasma membrane damage after shear force application, styryl dye FM 1-43 (Invitrogen—Thermo Fisher Scientific, Massachusetts, USA) was added to the hydrogel at a concentration of 5 $\mu g\ ml^{-1}$ immediately before mixing with cells. FM 1-43 was not added to the hydrogel when cell viability or proliferation experiments were performed. Cells were trypsinized and centrifuged (20 g, 5 min) before being mixed into the hydrogel at a final concentration of 1–2 $\times\ 10^6$ cells ml^{-1}. Bioprinting was performed using a custom-made bioprinter [7] at different flow rates through a stainless steel needle with an ID of 200 μm and a length of 12.7 mm (Nordson EFD, East Providence, USA). To obtain cylindrical constructs of a defined volume, the bioink was printed or cast into plastic rings (Shapeways, New York, USA). Alginate- or GelMA-based samples were crosslinked for 10 min with 0.1 M $CaCl_2$-solution or 1 min at 405 nm UV light, respectively. After crosslinking, FM 1-43 samples were fixed using

4% paraformaldehyde for 15 min before addition of DPBS and confocal imaging of FM 1-43. In cell viability experiments, samples were either treated directly after crosslinking with live/dead staining solution, or cultured in cell culture medium at 37 °C, 5% CO_2, 95% humidity until further use. To monitor cell proliferation, printed samples were not crosslinked but dissolved in cell culture medium and plated on cell culture dishes (0.5×10^6 cells per 56.7 cm^2), so that the cells could sink down and adhere to the bottom of the dish. Cells were passaged and reseeded at the same density every second day.

2.6. FM 1-43 fluorescence intensity evaluation

Microscopic imaging of printed constructs for FM 1-43 fluorescence intensity analyses was performed immediately after the bioprinting experiment on an upright Leica SP5X laser scanning confocal microscope (Leica, Wetzlar, Germany) with a 20×/1.0 numerical aperture (NA) water immersion objective lens. Image z-stacks were recorded over 160 μm sample depth at 2 μm z-section distance and 488 nm wavelength. For image analysis, stacks were maximum z-projected using ImageJ [26]. The mean FM 1-43 fluorescence intensity was determined for each cell using the software Clickpoints [27].

2.7. Cell proliferation and viability

Cell viability was determined immediately and 24 h after bioprinting. Live/dead staining solution containing ethidium homodimer-1 (EthD; Thermo Fisher Scientific, Massachusetts, USA) and calcein AM (eBioScience—Thermo Fisher Scientific, Massachusetts, USA) was prepared by suspending 1 μM calcein and 2 μM EthD in DPBS. Samples were incubated with the live/dead staining solution for 45 min at 37 °C, 5% CO_2, 95% humidity. After incubation, confocal image stacks covering 120–160 μm sample depth at 2 μm z-spacing were taken at 488 nm and 543 nm wavelengths on an upright Leica SP5X laser scanning confocal microscope (Leica, Wetzlar, Germany) with a 20×/1.0 NA water immersion objective lens. Before image quantification, images were maximum-intensity projected using ImageJ [26]. Cell proliferation was determined using FastFUCCI-expressing NIH/3T3 cells one day, three days, or seven days after the bioprinting experiment. After bioprinting, cells were seeded at a density of 0.5×10^6 cells per 56.7 cm^2 on tissue culture dishes to monitor the colour of the nuclei using an epifluorescence microscope (Leica DMI 6000 B, Leica, Wetzlar, Germany), equipped with a 20×/0.4 NA dry objective lens and a 0.5 coupler (10× effective magnification) and a charge-coupled device (CCD) camera (Hamamatsu Orca ER). Image quantification was performed on maximum projected (live/dead) or single plane images (proliferation), using the CellCounter Plugin from ImageJ [26].

2.8. Spinning disk shear force application

Cells were cultured on non-coated cell culture dishes for 24 h prior to the assay. The dishes were fixed in a customized microscope stage consisting of a compressed air-driven, rotating glass plate as described previously [28]. The glass plate was located 100 μm above the culture dish and rotated at increasing speed up to 1500 rpm for a total time of 30 s to apply increasing amounts of shear stress. During spinning, the cells were simultaneously imaged in bright-field and epifluorescence mode (488 nm exc.) to visualize the cells and FM 1-43 fluorescence. Imaging was performed at a frame rate of 5 s^{-1} with a 40×/0.6 NA dry objective.

2.9. Cell imaging in a microfluidic channel

NIH/3T3 cells (0.8 Mio ml^{-1}–1.25 Mio ml^{-1}) were harvested and mixed into a 3% alginate or 3% alginate solution containing 1.9 mM $CaCl_2$ and FM 1-43 (5 μg ml^{-1}). Under 6 bar (NIH/3T3) or 5 bar (A125, MDA-MB-231, hiPSC, HUVEC/Tert2) pressure application, the cell-laden bioink was injected into a polymethylmetacrylate microfluidic channel of 58 mm length with a quadratic cross section of 200 μm × 200 μm (Darwin Microfluidics, France) via a silicon tube ($l = 15$ cm; ID: 1 mm) (Darwin Microfluidics, France) [7]. During the channel passage, cells were imaged at high speed (500 fps) at the midsection of the channel, using a 40×/0.6 NA dry objective on an epifluorescence microscope (Leica DM IL, Leica, Wetzlar, Germany) equipped with a complementary metal-oxide semiconductor (CMOS) camera (acA720-520um, Basler, Germany) and a 100 mW diode laser (473 nm) in the bright-field and epifluorescence mode. For each recording, the velocity profile, shear rate profile, cell mechanical parameters (stiffness and fluidity) and hydrogel rheology (zero-shear-stress viscosity, characteristic shear rate for the onset of shear thinning, and shear-thinning exponent) were measured as previously described [29].

2.10. Statistical analysis

Unless otherwise stated, all experiments were repeated for at least three times. Statistical analysis was performed using Graphpad Prism 9.0.2 (GraphPad Software, San Diego, California USA). Differences between multiple groups and different treatments were analysed using two-way ANOVA followed by Šídák's multiple comparisons test. The two factors for the statistical analysis of live/dead experiments were pressure application (Ctrl vs 6 bar) and calcium addition (−Ca vs +Ca). Differences between two groups were determined using a Student's t-test. Statistical differences are indicated as follows: $^{*}p < 0.05$, $^{**}p < 0.01$, $^{***}p < 0.001$.

3. Results

3.1. Styryl dye-based visualization of shear stress induced plasma membrane damage

To visualize plasma membrane damages in cells during bioprinting, we applied the styryl dye FM 1-43,

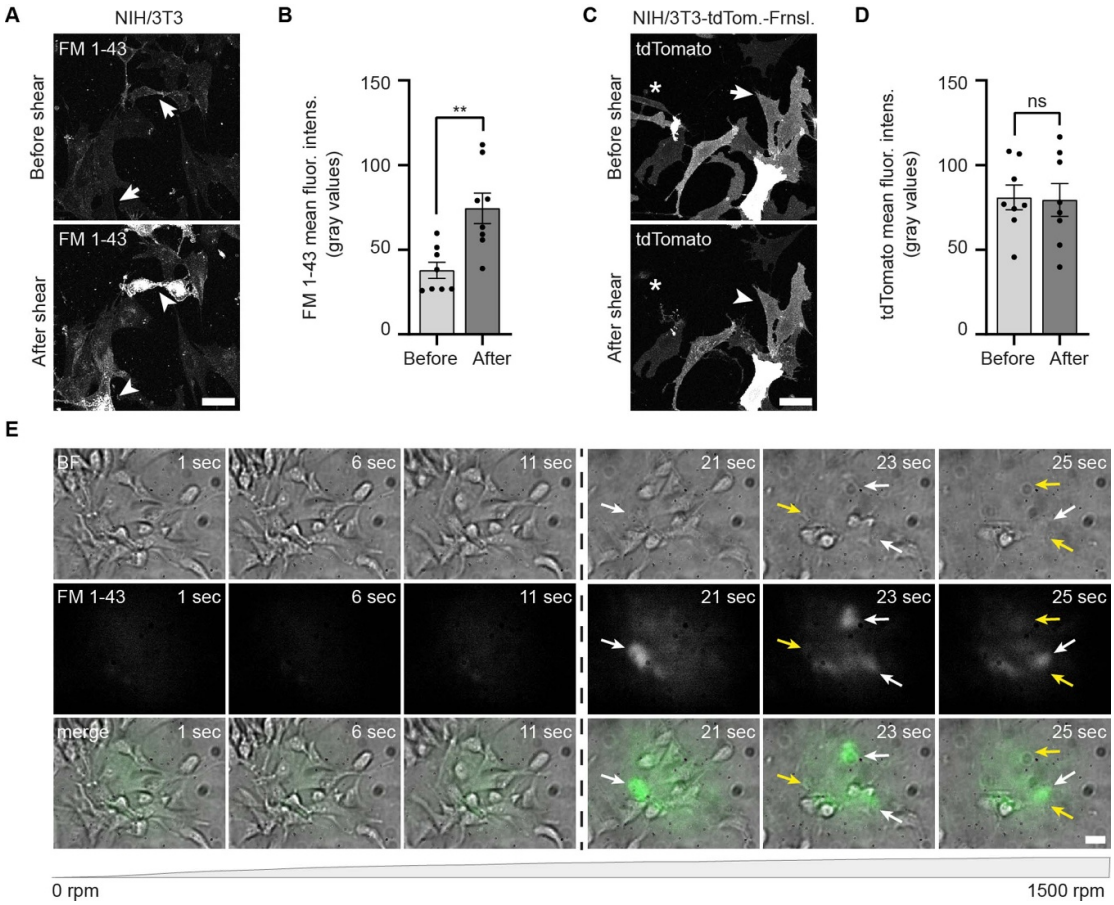

Figure 1. Incorporation of styryl dye FM 1-43 can be used to visualize shear stress-induced plasma membrane damage. (a) Confocal images of FM 1-43 stained NIH/3T3 fibroblasts seeded on fibronectin-coated cell culture dishes (upper panel). Cells displayed an increased FM 1-43 fluorescence intensity after being sheared by a coverslip (lower panel). Arrows and arrowheads mark the same cells in both panels. Scale bar: 50 μm. (b) Corresponding quantification of mean fluorescence intensities of non-sheared vs sheared NIH/3T3 fibroblasts stained with FM 1-43. $n = 8$ dishes, pooled from three biological replicates; error bars: sem; $^{**}P < 0.01$, student's t test; (c) Confocal images of NIH/3T3 cells stably expressing plasma membrane-targeted farnesylated tdTomato protein, seeded on fibronectin-coated cell culture dishes (upper panel). Application of shear stress similar as in (a) led to partial detachment of cells (asterisk) but did not increase tdTomato fluorescence intensity (lower panel). Arrows and arrowheads mark the same cells in both panels. Scale bar: 50 μm. (d) Corresponding quantification of mean fluorescence intensities of non-sheared vs. sheared NIH/3T3-tdTomato-Farnesyl cells. $n = 8$ dishes, pooled from three biological replicates; error bars: sem. (e) Live bright-field (BF, upper panel) and epifluorescence (FM 1-43, middle panel) imaging at different time points of FM 1-43-stained NIH/3T3 fibroblasts on a microscope stage-mounted spinning disk device at increasing shear stress up to 1500 rpm induced by a laminar flow. Note increase in FM1-43 fluorescence intensity (white arrow) immediately prior to cell detachment (yellow arrow). Scale bar: 25 μm.

which is non-fluorescent in aqueous solution but becomes brightly fluorescent upon excitation with blue light after incorporation into a lipid bilayer [30]. Since FM 1-43 integrates into the outer bilayer leaflet only, without crossing the bilayer, we hypothesized that it will specifically stain the plasma membrane when a cell is intact, whereas plasma membrane damage will allow FM 1-43 to enter the cell and incorporate also into internal membrane systems, resulting in an increased fluorescence intensity. To verify this, we imaged live NIH/3T3 cells via confocal microscopy in the presence of FM 1-43 before and immediately after the application of high shear stress by placing a coverslip on top of the culture and moving it under slight pressure. Non-sheared cells displayed an intact morphology, visualized by FM 1-43 plasma membrane staining of moderate intensity (figure 1(a), arrows). In contrast, sheared cells showed a significantly increased FM 1-43 fluorescence intensity (figure 1(a), arrowheads; figure 1(b)). To exclude that changes in FM 1-43 fluorescence intensity resulted from folding of the plasma membrane due to mechanical perturbation of the cells, we similarly sheared lentiviral NIH/3T3-tdTomato-Farnesyl reporter cells. Similar to FM 1-43 stained parental NIH/3T3 cells, they displayed an intact morphology prior to shear force application, but showed partial disruption after shear application (figure 1(c), asterisks). Importantly, shear force application was not associated with higher tdTomato fluorescence intensity (figure 1(c), arrowheads; figure 1(d)), indicating that the increased FM 1-43 fluorescence intensity after shear (figure 1(a)) was the

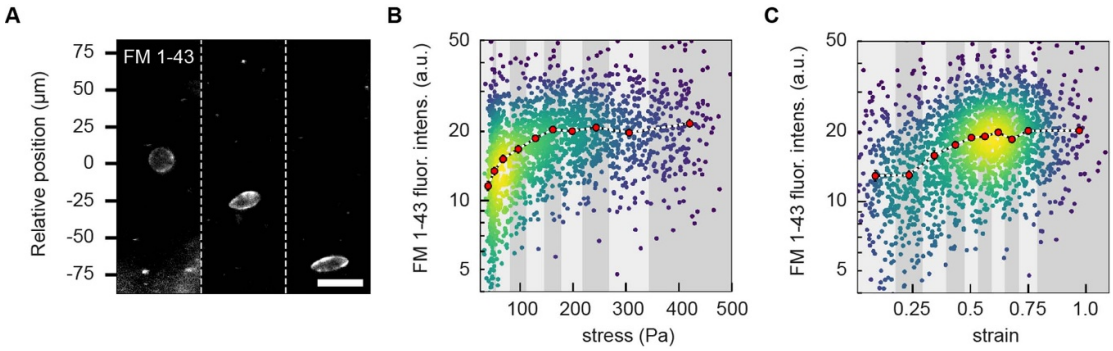

Figure 2. FM 1-43 fluorescence intensity correlates with cell elongation and imposed shear stress. Panel (a)–(c) show representative data from one out of four biological replicates. (a) Epifluorescence images of FM 1-43-stained fibroblasts in 3% alginate at different positions in a 200 μm ID and 58 mm length capillary. Cells were measured approx. 29 mm downstream of the channel inlet at 6 bar pressure application. Note increased FM 1-43 fluorescence intensity of cells closer to the channel wall (-75 μm) compared to cells in the channel centre (0 μm). Scale bar: 30 μm. (b), (c) FM 1-43 fluorescence intensity versus shear stress (b) or cell strain (c) for NIH/3T3 cells during capillary passage, measured as described in (a). Each data point corresponds to the average stress (b) or strain (c) and FM 1-43 fluorescence intensity of a single cell. Trends in regions with overlapping data points are displayed by colours, indicating the Gaussian kernel density. Red data points are median values computed for ten bins containing an equal number of cells. Bin boundaries are indicated by the light/dark grey background.

result of *de novo* dye incorporation into intracellular membrane surfaces.

Since cells during bioprinting experience shear stress under laminar flow conditions, we next tested whether FM 1-43 uptake could also be triggered by laminar flow-induced shear stress. To this end, we imaged live NIH/3T3 fibroblasts via epifluorescence microscopy in the presence of FM 1-43 at continuously increasing, laminar flow-induced shear stress, applied by a microscope-stage mounted spinning disk device [28]. When flow-induced shear stresses were slowly increased, cellular FM 1-43 fluorescent intensity levels remained constant (figure 1(e), supplementary movie). However, immediately prior to flow-induced detachment of the cells from the substrate (figure 1(e), yellow arrows, supplementary movie), we observed a sudden increase in cellular FM 1-43 intensity (figure 1(e), white arrows; supplementary movie), suggesting that the plasma membrane disrupted prior to or during cell detachment, resulting in a sudden exposure of large intracellular membrane surface area and increased FM 1-43 incorporation. Together, these data show that FM 1-43 is suitable to monitor plasma membrane damages in cells exposed to shear stress.

3.2. FM 1-43 intensity increases as a function of shear stress and strain

To test whether FM 1-43 also allows us to visualize plasma membrane damages under the typical flow conditions in a printing needle during biofabrication, we subjected NIH/3T3 cells ($0.8–1.25 \times 10^6$ ml^{-1}) suspended in 3% alginate containing FM 1-43 to laminar flow using a custom-designed microfluidic cell deformation cytometer (figure S1—supplementary information) [7, 29]. During capillary passage (6 bar), cells were imaged in bright-field and epifluorescence mode (473 nm) at high temporal resolution (500 Hz, 30 μs exposure time). This allowed us to directly monitor the fluorescence intensity and strain of each cell and its position in the channel. Knowing the corresponding fluid shear stress profile along the radial position for our capillary geometry and pressure (figure S2(a)—supplementary information), we were able to calculate the imposed shear stress for each cell. As expected, we found that the FM 1-43 fluorescence intensity of the cells increased with their relative position toward the channel wall, where the shear stress is highest (figures 2(a) and (b)). Importantly, FM 1-43 intensity increased approximately linearly with the shear stress-induced cell strain (figure 2(c)). These data demonstrate that cellular FM 1-43 incorporation is suitable to monitor shear stress- and strain-induced plasma membrane disruption in a shear thinning material under three-dimensional (3D) laminar flow conditions.

3.3. FM 1-43 can be applied in bioprinting experiments to visualize plasma membrane disruptions

We next tested whether FM 1-43 was also suitable to visualize the effects of shear stress on plasma membrane integrity in extrusion bioprinting experiments. We suspended NIH/3T3 fibroblasts (1×10^6 ml^{-1}) in 2% alginate containing FM 1-43, either cast or printed them by applying a high pressure of 6 bar through a 12.7 mm long needle of 200 μm ID, corresponding to a maximal shear stress of 2500 Pa at the needle wall (figure S2(b)—supplementary information), and subsequently imaged the samples by confocal microscopy. In both, cast control and printed samples, cells exhibited a round morphology (figure 3(a)). Cells in control samples predominantly showed a moderate FM 1-43 fluorescence

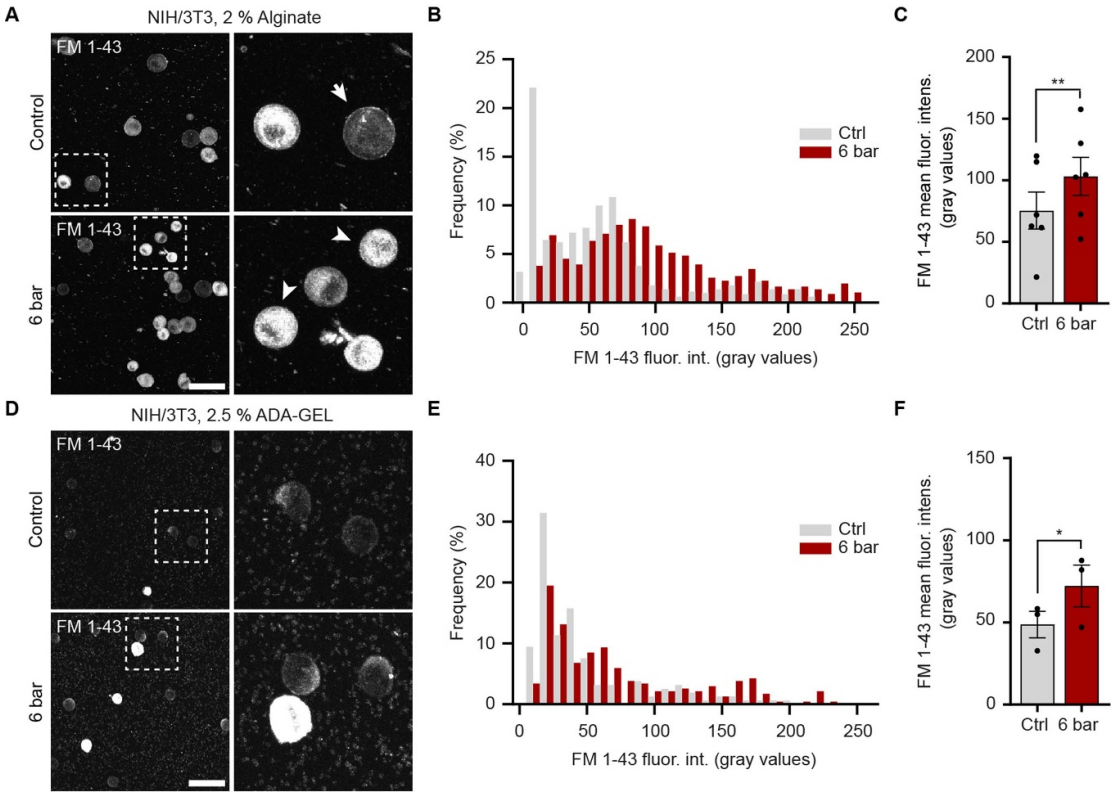

Figure 3. Extrusion bioprinting-induced shear stress leads to increased uptake of FM 1-43 in NIH/3T3 fibroblasts. (a) Confocal image stacks (max. projection) of NIH/3T3 fibroblasts in 2% alginate cast or printed at 6 bar pressure. Scale bar: 50 μm. (b) Histogram of mean FM 1-43 fluorescence intensities of cast control (grey) or printed samples (6 bar, red) in 2% alginate. $n = 6$ biological replicates. (c) Quantification of mean fluorescence intensities of FM 1-43 as shown in (b). $n = 6$ biological replicates; error bars: sem; $^{**}P < 0.01$, paired student's t test. (d) Confocal image stacks (max. projection) of NIH/3T3 fibroblasts cast or printed at 6 bar pressure in 2.5% ADA-GEL. Scale bar: 50 μm. (e) Histogram of mean FM 1-43 fluorescence intensities of cast control (grey) or printed samples (6 bar, red) in 2.5% ADA-GEL. $n = 3$ biological replicates. (f) Quantification of mean FM 1-43 fluorescence intensities as shown in (e). $n = 3$ biological replicates; error bars: sem; $^{*}P < 0.05$; paired student's t test.

intensity, characterized by a brighter rim around the cell perimeter (figure 3(a), arrow), indicative of plasma membrane staining. In contrast, printed cells predominantly showed a high fluorescence intensity throughout the whole cell (figure 3(a), arrowheads), indicating that both plasma membrane and intracellular membrane systems were stained by FM 1-43 after entering the cells. Consistent with this, the distribution of the mean fluorescence intensity per cell was shifted from lower to higher intensities in printed compared to control samples (figure 3(b)), resulting in a significant increase in the mean FM 1-43 fluorescence intensity (figure 3(c)). To exclude that the increased FM 1-43 uptake in response to shear stress was related to the lack of cell adhesion motives in alginate, we repeated the experiments in 2.5% ADA-GEL. As in alginate, confocal imaging revealed a round cell morphology, an increased number of bright cells after 6 bar pressure application (figures 3(d) and (e)), and a significant increase in cellular FM 1-43 mean fluorescence intensity in printed compared to control samples (figures 3(e) and (f)). These data show that shear stress-induced plasma membrane damages during bioprinting can be visualized by incorporation of the styryl dye FM 1-43.

3.4. High shear stress results in cell damage and impaired cell survival

We next tested whether shear force-induced plasma membrane damage affects cell viability. NIH/3T3 fibroblasts (2×10^6 ml^{-1}) were immersed in 2% alginate solution and cast or printed through a 200 μm stainless steel needle at high (6 bar) pressure. Confocal microscopy of calcein/EthD-based live/dead staining immediately (day 0, d0) or 24 h after extrusion-based bioprinting (day 1, d1) revealed the presence of three distinct groups of stained cells. Live cells exhibited a round morphology with homogeneous calcein dye distribution (figure 4(a), upper panel). By contrast, dead cells showed intense red staining of the nucleus by EthD-1 (figure 4(a), lower panel, asterisk) and residual, granulated calcein staining, indicating the presence of vesicles with remaining metabolic activity (figure 4(a), arrow). Interestingly, we found a third group of cells resembling the vesicular calcein-staining of dead cells, but lacking EthD staining (figure 4(a), middle panel, arrows). Cells in this group were counted as 'damaged'. In control samples, the majority of cells showed a homogeneous distribution of calcein staining on the same day of the bioprinting experiment (figure 4(b), arrow),

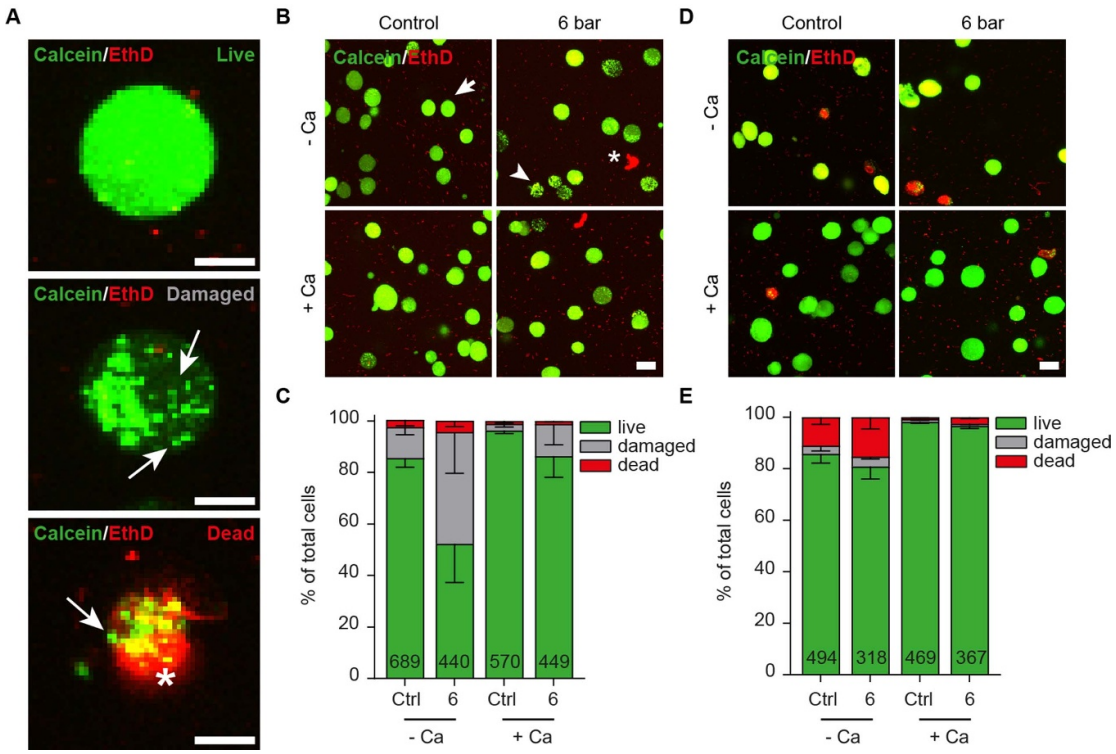

Figure 4. Shear stress-induced decrease in cell survival can be prevented by supplementation of the hydrogel with physiological concentrations of $CaCl_2$. (a) Calcein/ethidium homodimer (EthD)-based live/dead staining of NIH/3T3 fibroblasts in 2% alginate. Live cells (upper panel) show homogeneous calcein distribution. Cells with granular-like calcein staining of remaining vesicles (arrow) but no EthD staining are counted as damaged (middle panel). Red nuclear EthD staining marks dead cells (lower panel, asterisk) accompanied by some residual vesicular calcein (arrow). Scale bar: 10 μm. (b) Confocal image stacks (max. projections) of cells cast (Ctrl) or printed (6 bar) in 2% alginate or 2% alginate supplemented with 1.9 mM $CaCl_2$. Samples were stained with calcein/EthD and imaged immediately after bioprinting (d0). Note damaged (arrowhead) and dead (asterisk) cells. Scale bar: 20 μm. (c) Quantification of the mean fractions of live, dead, or damaged cells as described in (b). Numbers at the bottom of the bars indicate the mean number of total cell counts. $n = 5$ biological replicates; error bars: sem. (d) Confocal image stacks (max. projections) of cells cast (Ctrl) or printed (6 bar) in 2% alginate or 2% alginate with 1.9 mM $CaCl_2$. Samples were stained with calcein/EthD and imaged 24 h after bioprinting (d1). Scale bar: 20 μm. (e) Quantification of the mean fractions of live, dead, or damaged cells as described in (d). $n = 5$ biological replicates; error bars: sem.

corresponding to ~85% of live cells (figure 4(c)). In contrast, application of high (6 bar) pressure increased the number of damaged (figure 4(b), arrowhead) and dead cells (figure 4(b), asterisk), resulting in a significant reduction of cell survival to 52% (figure 4(c), table S1—supplementary information). These data confirm that printing-induced shear stress can cause considerable cell damage and immediate cell death. Live/dead staining 24 h after the experiment revealed a reduced total cell number in all samples compared to samples on the day of printing (figures 4(c) and (e)), suggesting that damaged cells died and were no longer detectable after 24 h. Consistent with this, the fraction of dead cells increased in all samples, while the fraction of damaged cells decreased (figures 4(c) and (e)). Surprisingly, the strong pressure-induced reduction of the live cell fraction observed immediately after printing was hardly visible after 24 h, with 85% (control) and 81% (6 bar) live cells (figure 4(e)), suggesting that not all damaged cells died during the first 24 h after printing, or that additional effects independent of the bioprinting process may have influenced cell survival in alginate (figure 4(d), top panel and (e)). These data demonstrate that the application of bioprinting-induced shear stress can lead to considerable cell damage and reduction in cell survival. Together with our previous results, this strongly suggests that shear stress-induced damage to the plasma membrane can cause cell damage and death.

3.5. Calcium chloride can rescue shear stress induced cell damage and cell death

Considering the role of calcium ions on plasma membrane repair mechanisms [22, 23], we next tested whether the presence of extracellular calcium during the bioprinting process affects the cellular shear stress vulnerability. As described above, NIH/3T3 fibroblasts suspended in $CaCl_2$-supplemented alginate were either cast (control) or printed at high pressure using a dispensing needle of 200 μm ID and live/dead-stained on day 0 or day 1 after bioprinting. Nearly all cells in control samples showed a homogeneous calcein distribution (figure 4(b), lower panel), which corresponded to ~96% live cells (figure 4(c)). Notably, even 6 bar pressure only moderately reduced the cell viability to 86% (figure 4(c)),

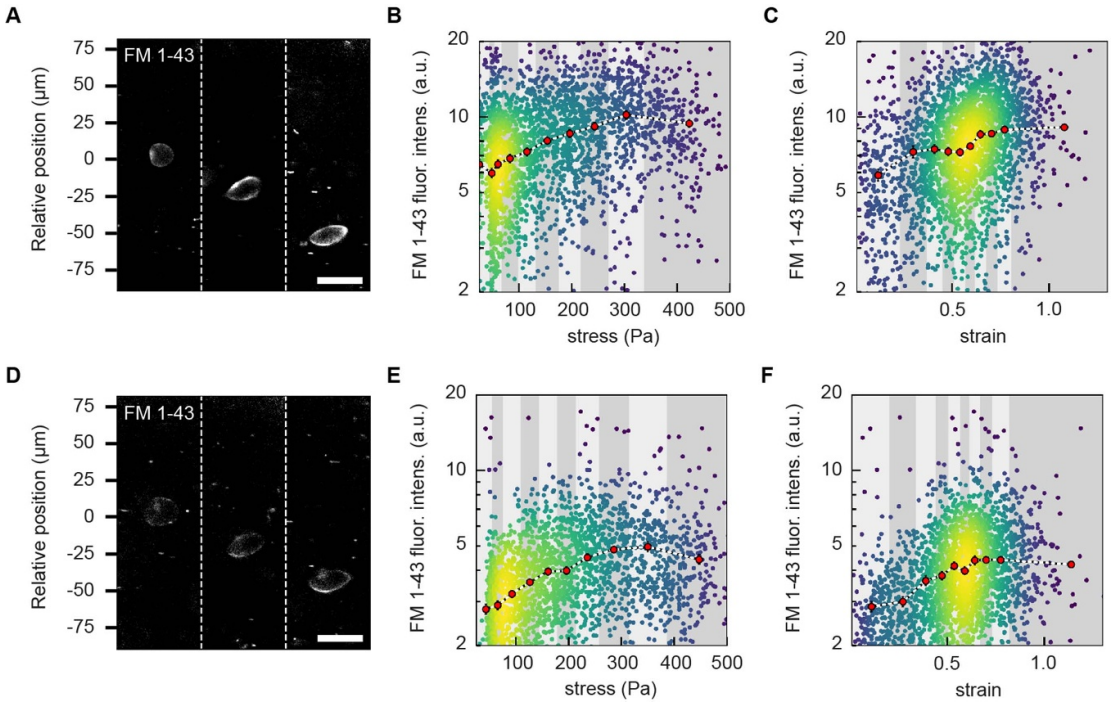

Figure 5. NIH/3T3 cells passing through a deformation cytometer display a lower FM 1-43 fluorescence intensity, when the bioink is supplemented with $CaCl_2$. Panels (a)–(f) show representative data of 3 biological replicates. (a) Epifluorescence images of FM 1-43-stained NIH/3T3 fibroblasts in 3% alginate at different positions in a microfluidic capillary of 200 μm ID and 58 mm length. Cells were measured approx. 29 mm downstream of the channel inlet at 6 bar pressure application. Note increased FM 1-43 fluorescence intensity of cells closer to the channel wall (−75 μm) compared to cells in the channel centre (0 μm). Scale bar: 30 μm. (b), (c) FM 1-43 fluorescence intensity versus shear stress (b) or cell strain (c) for NIH/3T3 cells during capillary passage, measured as described in (a). Each data point corresponds to the average stress (b) or strain (c) and FM 1-43 fluorescence intensity of a single cell. Trends in regions with intersecting data points are displayed by colours, which indicate the Gaussian kernel density. Red data points are median values computed for ten bins containing an equal number of cells. Bin boundaries are indicated by the light/dark grey background. (d) Epifluorescence images of FM 1-43-stained NIH/3T3 fibroblasts in 3% alginate supplemented with $CaCl_2$ measured as described in (a). Note the lower FM 1-43 fluorescence intensity of the cells when positioned toward the channel wall (−75 μm) as compared to non-calcium supplemented alginate (a). Scale bar: 30 μm. (e), (f) Corresponding FM 1-43 fluorescence intensity versus shear stress (e) or cell strain (f) relationship for NIH/3T3 cells in $CaCl_2$-supplemented alginate.

resulting in a significant increase in cell survival of more than 30% (6 bar), compared to the cell survival in alginate without calcium (figure 4(c); table S1—supplementary information). As in non-calcium-supplemented samples, we counted reduced total cell numbers and a strongly reduced pressure-dependency of the effects on cell viability on day 1, with 98% (control) and 96% (6 bar) viable cells (figures 4(d) and (e)). Importantly, on day 1, control samples showed a strong cell survival, and 6 bar samples showed a significantly improved cell survival compared to non-calcium-supplemented samples on day 1 (figure 4(e); table S1—supplementary information), suggesting that calcium has additional, shear stress-independent effects on cell survival in alginate. These results demonstrate that the addition of physiological levels of extracellular calcium to the hydrogel can significantly reduce the harmful effects of shear stress on cell survival during extrusion-based bioprinting.

To investigate whether calcium improved the cellular shear stress vulnerability by promoting plasma membrane resealing, we compared the fluorescence intensities of FM 1-43-stained NIH/3T3 cells suspended in alginate or $CaCl_2$-supplemented alginate in the deformation cytometer. Bright-field and epifluorescence (473 nm) imaging mode of both cells suspended in pure and $CaCl_2$-suspended alginate revealed higher FM 1-43 fluorescence intensities with an increased radial position toward the channel wall (figures 5(a) and (d)) and a correlation of FM 1-43 fluorescence intensity with shear stress (figures 5(b) and (e)) and cell strain (figures 5(c) and (f)). Importantly, FM 1-43 fluorescence intensities were much lower in $CaCl_2$-supplemented compared to pure alginate (figures 5(a)–(f)), demonstrating that $CaCl_2$-supplementation of the hydrogel can reduce shear stress-induced damage of the plasma membrane.

3.6. Shear stress induced cell damage and death, and $CaCl_2$-mediated cell protection increase with lower cell stiffness

Since the sensitivity of cells to fluid shear stress has been suggested to vary between cell types due to differences in their mechanical properties [31], we repeated our deformation cytometer and bioprinting experiments with A125, MDA-MB-231 breast cancer

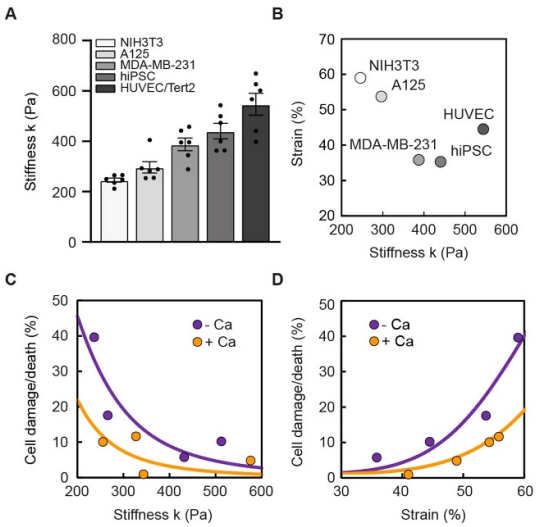

Figure 6. Cell death and calcium-dependent cytoprotection depend on cell stiffness and cell strain during needle passage. (a) Deformation cytometer-based quantification of the stiffness of NIH/3T3, A125, MDA-MB-231, hiPSC and HUVEC/Tert2. Cells suspended in 3% alginate with or without 1.9 mM $CaCl_2$ were injected into a capillary (5.8 cm, 200 μm ID) at 5 bar pressure. $n = 6$ biological replicates; error bars: sem. (b) Cell strain over stiffness for the indicated cell types, measured in the deformation cytometer. (c), (d) Bioprinting shear stress-induced cell damage/death on day 0 (normalized on cell damage/death of non-printed control samples for each cell type) over cell stiffness (c) and strain (d) for different cell types. Data points from left to right: NIH/3T3, A125, MDA-MB-231, HUVEC/Tert2 (c); HUVEC/Tert2, MDA-MB-231, A125, NIH/3T3 (d). Data were fitted using the Hill-equation, $n = 3$ independent biological replicates per data point.

cells, hiPSC, and HUVEC/Tert2 endothelial cells, all of which exhibited different stiffnesses (figure 6(a)).

The deformation cytometer experiments showed for all cell types an increase in FM 1-43 fluorescence intensity with increasing shear stress and cell strain, similar to what we observed in NIH/3T3 cells (figure S3(a)–(h)—supplementary information). Cell membrane damage in response to shear stress, as monitored by the increase in FM 1-43 fluorescence intensity, tended to be more pronounced in softer cells (A125, MDA-MB-231) compared to stiffer cells (hiPSC, HUVEC/Tert2), indicating that not primarily the shear stress but the resulting cell strain causes membrane damage. When we supplemented the alginate solution with 1.9 mM $CaCl_2$, the membrane damage was reduced compared to non-calcium-supplemented samples in all cell types except the stiffest ones (HUVEC/Tert2), which showed hardly any membrane damage regardless of $CaCl_2$-supplementation (figure S3—supplementary information).

When we examined the effects of bioprinting on cell viability, we found that the supplementation of a 2% alginate solution with 1.9 mM $CaCl_2$ improved both immediate and long-term survival of cells in control samples and samples printed at 6 bar pressure application (figure S4—supplementary information). The extent of this Ca^{2+}-rescue effect on cell survival was smaller in stiffer cells in absolute terms, as stiffer cells tended to survive better and showed less membrane damage in response to shear stress (figures S3 and S4—supplementary information). We hypothesized that an increased stiffness reduced the deformation of cells during needle passage, thus reducing cell damage and subsequent cell death. Indeed, our deformation cytometer experiments revealed a lower average strain in stiffer cell types (figures 6(a) and (b)) under otherwise identical conditions. Consistent with our hypothesis, cell damage and death decreased with increasing cell stiffness, but increased with cell strain (figures 6(c) and (d)). Importantly, calcium-supplementation reduced cell damage and death not only for soft cells but also for stiff cells by roughly two-fold (figures 6(c) and (d)). Taken together, these data demonstrate that shear stress-induced cell damage and death during bioprinting in alginate are dependent on cell stiffness and strain, and that alginate supplementation with physiological concentrations of $CaCl_2$ can increase cell survival by reducing the detrimental effects of plasma membrane damage during cell deformation.

3.7. Application of shear stress has no effect on cell proliferation

To determine whether bioprinting-induced shear stress or calcium-supplementation of the hydrogel affected the long-term behaviour of the cells, we monitored the cell proliferation of cast and bioprinted cells over a seven-day period using FUCCI cell cycle sensor-expressing NIH/3T3 fibroblasts. Serum-starvation of NIH/3T3 FUCCI-reporter cells cultured in two-dimensional (2D) culture dishes revealed a significantly reduced cell proliferation in the absence of serum as compared to full serum levels (figures S5(a) and (b)—supplementary information), demonstrating that the FUCCI-system is responsive to proliferative cues in NIH/3T3-cells.

To investigate the effects of pressure-induced shear stress on the proliferation of the surviving cells independently of the hydrogel matrix, we re-seeded the cells on 2D cell culture dishes after printing in non-gelated alginate with or without $CaCl_2$. We counted kusabira-orange-cdt1 (red) or azami green-geminin (green) expressing nuclei one day (figure 7(a)), three days (figure S5(c)—supplementary information) or seven days (figure S5(e)—supplementary information) post-printing to quantify cell proliferation. In line with our data on cell viability, we observed reduced cell numbers after high pressure application on day 1 after bioprinting. However, this effect was not visible at later time points, suggesting that the proliferative capacity of the cells was not affected by shear stress (figure 7(b); figures S5(d) and (f)—supplementary information). Consistent with this, the percentage of green nuclei,

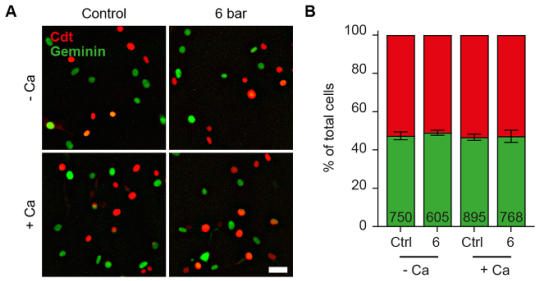

Figure 7. Bioprinting-related shear stress has no effect on the proliferation of surviving cells. (a) Epifluorescence images of FUCCI cell cycle expressing NIH/3T3 fibroblasts 24 h after bioprinting. Cells were either cast (Ctrl) or printed (6 bar) in 2% alginate (upper panel) or 2% alginate supplemented with 1.9 mM $CaCl_2$ (lower panel) and seeded on 2D culture dishes, after dissolving the non-gelled hydrogel in cell culture medium. Scale bar: 50 μm. (b) Mean fractions of green or red nuclei counts as described in (a). At the bottom of each bar, the mean total cell count is given. $n = 3$ biological replicates; error bars: sem.

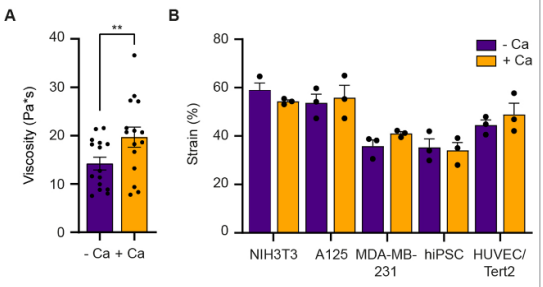

Figure 8. Supplementation of alginate with $CaCl_2$ leads to an increase in the viscosity of alginate but not to an increased cell strain under the same pressure. (a) Viscosity of 3% alginate (purple) or 3% alginate supplemented with 1.9 mM $CaCl_2$ (orange), measured in the cell deformation cytometer. $n = 15$ biological replicates. (b) Quantification of the average strain of NIH/3T3, A125, MDA-MB-231, hiPSC, HUVEC/Tert2 cells immersed in 3% alginate (purple) or 3% alginate supplemented with 1.9 mM $CaCl_2$. $n = 3$ biological replicates.

showing actively proliferating cells in the G2 phase of the cell cycle, was close to 50% in both control and printed samples of pure alginate on day 1, 3 and 7 (figures 7(b) and S5(d), (f)—supplementary information), demonstrating that cell proliferation was not affected by printing-related shear stress. Similarly, the proportion of green nuclei was not affected by calcium supplementation (figures 7(a), (b) and S5(d)–(f)—supplementary information). Together with our previous data, this indicates that bioprinting-induced shear stress, despite its detrimental effects on immediate and long-term cell viability, does not affect the proliferative capacity of surviving cells. Furthermore, calcium-supplementation has no detrimental effect on cell proliferation.

3.8. Calcium chloride rescues shear stress induced cell damage and cell death in GelMA

Since alginate-based bioinks are crosslinked by Ca^{2+}-ions, we tested whether the cytoprotective effect of $CaCl_2$ was caused by an altered bioink rheology, rather than by cell intrinsic effects. Using our deformation cytometer setup, we found that supplementation of 3% alginate with 1.9 mM $CaCl_2$ significantly increased the viscosity (figure 8(a)). Since an increased viscosity of alginate bioinks has previously been suggested to reduce cell deformation during bioprinting by shifting its flow pattern from a quadratic parabola to a plug-flow behaviour [17], we compared the cell deformation of NIH/3T3, A125, MDA-MB-231, hiPSC and HUVEC/Tert2 cells in non-supplemented and calcium-supplemented alginate (3%). This revealed that the cell deformation was not decreased in $CaCl_2$-supplemented compared to non-supplemented alginate (figure 8(b)). Notably, some cell lines showed even a slightly increased cell strain in $CaCl_2$-supplemented compared to pure alginate, suggesting that the protective effect of calcium was not caused by an altered flow behaviour of the alginate hydrogel.

To further investigate this, we repeated the experiments in 9% GelMA, which is crosslinked by UV light and not $CaCl_2$ [32]. Similar to the experiments in alginate, calcein/EthD-based live/dead staining revealed three groups of cells in GelMA: live cells with homogeneous calcein dye distribution, dead cells with nuclear red EthD and some residual vesicular calcein staining, and EthD-negative damaged cells with dead-cell resembling granule-like calcein staining (figure 9(a)). The majority of cells in cast control samples of GelMA without calcium displayed an intact round morphology immediately after the experiment, visualized by homogeneous calcein staining (figure 9(b)). By contrast, printed samples contained a larger number of EthD-positive dead cells as well as damaged cells (figure 9(b)) resulting in a reduction of cell viability from 99% (control) to 82% (6 bar) (figure 9(c)). When GelMA was supplemented with $CaCl_2$, cast control samples also showed an intact morphology and 99% cell viability (figures 9(b) and (c)). Importantly, cell viability in printed samples (96%) was not any longer reduced compared to cast samples, and increased by 14% compared to printed GelMA-samples without calcium. Twenty-four hours after bioprinting cell viability was reduced in printed (57%) compared to cast (78%) non-supplemented samples, while it was not reduced in printed (79%) compared to cast (84%) calcium-supplemented samples, accounting for a significant improvement of 22% in printed calcium-supplemented vs non-supplemented samples (figures 9(d) and (e); table S1—supplementary information). Hence, the protective effect of calcium supplementation against shear stress induced damages was persistent over time in GelMA. Interestingly, as opposed to our alginate-based data, neither non-supplemented nor Ca^{2+}-supplemented GelMA-samples displayed a

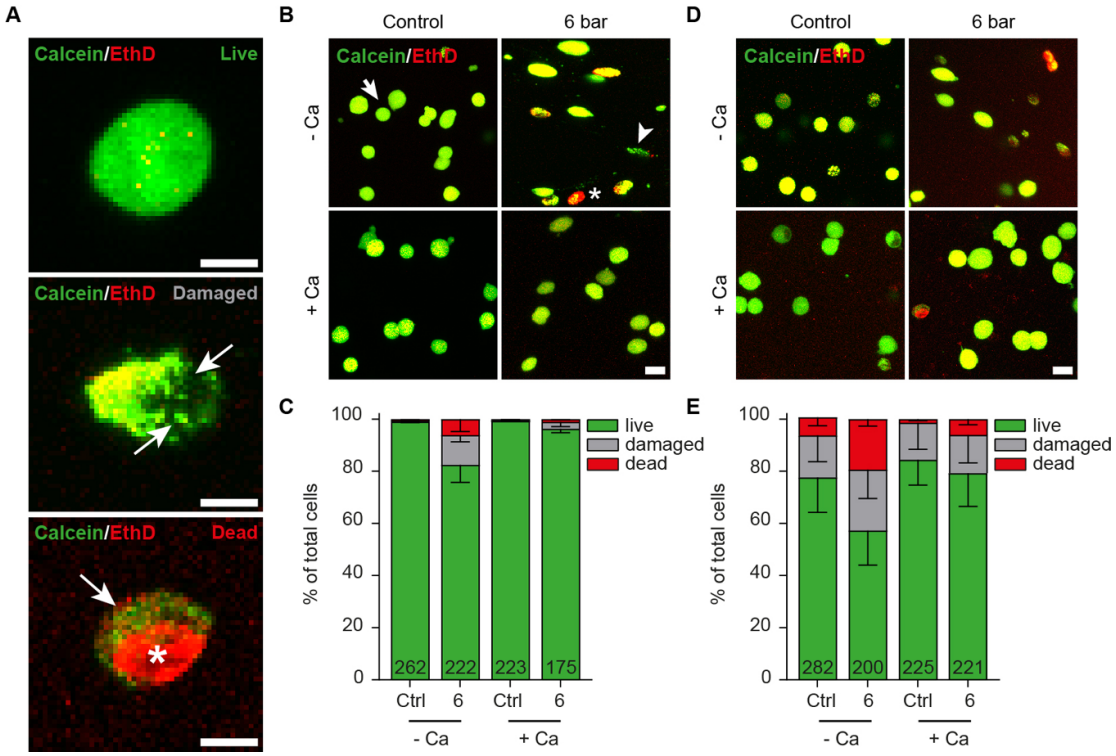

Figure 9. Calcium supplementation of methacrylated gelatin (GelMA) reduces detrimental effects of shear stress on cell survival. (a) Calcein/ethidium homodimer (EthD)-based live/dead staining in NIH/3T3 fibroblasts immersed in 9% GelMA. Similar to alginate, live cells (upper panel) show homogeneous calcein distribution, while dead cells can be distinguished by red nuclear EthD staining (lower panel, asterisk) accompanied by residual vesicular calcein (arrow). Damaged cells display similar granular calcein staining of remaining vesicles (arrow) but no nuclear EthD staining (middle panel). (b) Confocal image stacks (max. projection) of NIH/3T3 cells, which were cast (Ctrl) or printed (6 bar) in 9% GelMA or 9% GelMA supplemented with 1.9 mM $CaCl_2$ and stained with calcein/EthD immediately after the bioprinting. Scale bar: 20 μm. (c) Quantification of the mean fractions of live, dead, or damaged cells as described in (b). Numbers at the bottom of the bars indicate the mean number of total cell counts per experiment. $n = 3$ biological replicates; error bars: sem. (d) Confocal image stacks (max. projection) of NIH/3T3 cells, which were cast (Ctrl) or printed (6 bar) in 9% GelMA or 9% GelMA supplemented with 1.9 mM $CaCl_2$ and stained with calcein/EthD 24 h after bioprinting. Scale bar: 20 μm. (e) Quantification of the mean fractions of live, dead, or damaged cells as described in (d). Numbers at the bottom of the bars indicate the mean number of total cell counts per experiment. $n = 3$ biological replicates; error bars: sem.

reduced total cell count after 24 h (figures 9(c) and (e)), suggesting that shear stress-induced cell death was not masked by shear stress-independent effects in GelMA, whereas shear stress-dependent as well as shear stress-independent effects caused cell death in alginate.

Since cells in cast control alginate samples tended to show a reduced survival compared to cells cast in GelMA (figure 4(c), left bar; figure 9(c), left bar), we hypothesized that shear stress-independent cell damage or death in alginate may already have occurred during the cell suspension process. Hence, we directly compared the FM 1-43 intensity of cells in cast samples after suspension in alginate or GelMA. Consistent with our hypothesis, we found that the FM 1-43 baseline signal of cast samples was significantly higher in alginate compared to GelMA (figure S6—supplementary information). Together, these data demonstrate that the protective effect of calcium against shear stress-induced cell damage and death is not limited to alginate-based bioinks.

4. Discussion

Damage to the plasma membrane due to shear stress is a major cause of reduced cell survival in extrusion-printing based biofabrication. However, methods to monitor plasma membrane damage or to reduce the shear stress-vulnerability of cells are not well established. Here, we develop new assays to visualize plasma membrane damage, based on the enhanced membrane incorporation of the fluorescent styryl dye FM 1-43 in sheared versus non-sheared cells. Using our assays, we demonstrate that supplementation of bioinks with physiological concentrations of Ca^{2+} can efficiently reduce the adverse effects of bioprinting-induced shear stress on plasma membrane damage and cell survival.

Our results demonstrate that FM 1-43 can be used in bioprinting experiments to indicate shear stress-induced damage to the plasma membrane. Because FM 1-43 only inserts into the outer layer of the plasma

membrane without crossing it, measurement of FM 1-43 influx through lesions is widely used in studying membrane repair mechanisms [33]. It has been suggested that injury-induced uptake of FM 1-43 causes additional staining of intracellular cytoplasm-facing membrane leaflets, leading to increased cellular fluorescence intensity [34, 35].

Based on this, we hypothesized that FM 1-43 could be used to visualize shear stress-induced plasma membrane disruption during bioprinting. As expected, the dye stained the plasma membrane under control conditions, whereas application of shear stress to FM 1-43-stained cells resulted in increased fluorescence intensity in both 2D and 3D experimental setups. Importantly, cells stably expressing a tdTomato-farnesyl plasma membrane label did not exhibit increased tdTomato fluorescence intensity after application of shear stress, demonstrating that the changes in FM 1-43 fluorescence intensity were not due to plasma membrane staining but the result of increased cellular uptake. Similarly, we observed a shear stress-dependent uptake of FM 1-43 in microfluidic and extrusion bioprinting assays, demonstrating the suitability of FM 1-43 to monitor plasma membrane damage in bioprinting approaches.

Our microfluidic assay experiments have also shown that the fluorescence intensity of FM 1-43 stained cells not only correlates with the externally applied shear stress but is also sensitive to changes in cell strain. This makes the FM 1-43 based microfluidic assay a unique and powerful tool to study the interdependence between shear stress, cell deformation and cell damage, and to adapt bioprinting parameters accordingly. Microfluidic assays may be used to experimentally verify theoretical simulations of cell deformation to predict cell damage or to characterize cell type-specific critical stress or strain levels that inevitably lead to cell damage [36, 37].

Shear stress-induced cell deformations can cause plasma membrane damages that significantly impair cell viability and behaviour [15, 36, 37]. Consistent with this, we observe that higher pressures were associated with an increased cell damage and a reduced viability of NIH/3T3 fibroblasts. Interestingly, our deformation cytometer and bioprinting experiments using cell types of different stiffnesses revealed that these effects were less prominent in stiffer cell types. Moreover, stiffer cell types showed a reduced shear stress-induced cell deformation and FM-1 43 incorporation in our deformation cytometer. These results demonstrate that a high cell stiffness can protect cells from shear stress-induced deformation, plasma membrane damage, and subsequent cell death. Surprisingly, the proliferative capacity of the surviving cells was not affected by shear. It remains to be tested though, whether other cell physiological processes, such as motility, apoptosis, and gene expression are affected by bioprinting-induced shear stress.

Notably, measures to improve cell viability after extrusion bioprinting have mostly focused on modifying external parameters such as the bioink or nozzle design to reduce shear stress, rather than modifying the shear stress vulnerability of the printed cells [18, 19]. Since calcium has fundamental influence on different cellular processes such as cell signalling, vesicle transport and fusion, or cytoskeleton remodelling, which all affect the cell's response to wounding [20, 23, 38–40], we hypothesized that calcium may also affect the cellular response to shear stress-induced damage during extrusion bioprinting. Consistent with this, we found that supplementing the bioink with physiological concentrations of Ca^{2+} strongly improves cell survival in both bioinks we tested, alginate and GelMA. Importantly, the cytoprotective effect of calcium-supplementation was persistent in other cell types with different stiffnesses. We found that softer cells, which deform more under shear than stiffer ones, particularly benefited from calcium-supplementation. Importantly, like non-calcium-supplemented samples, also calcium-supplemented samples showed a clear dependency of cell damage and death on cell stiffness and strain. However, cell damage and death for a given cell type at a given strain was consistently reduced in the presence of calcium, roughly by two-fold compared to the shear stress-induced cell damage and death in the absence of calcium-supplementation. This demonstrates that calcium improves the cellular capability to cope with shear stress-induced deformation and plasma membrane damage.

To exclude that this cytoprotective effect was caused by a shift towards a plug flow behaviour of calcium-supplemented alginate and possibly a reduced cell strain, we compared the viscosity as well as cell strain between calcium- and non-calcium supplemented alginate in our deformation cytometer for otherwise identical conditions. Those experiments revealed an increased viscosity of calcium-supplemented alginate, but the cell strain was largely unaffected. Together with our observation that calcium also protected cells from shear stress-induced cell death in GelMA, these data indicate that the cytoprotective effect of calcium is not related to a change in hydrogel rheology.

We instead hypothesize that the cytoprotective effect of calcium is mediated by an improved resealing of the plasma membrane, triggered by passive calcium influx through the damaged membrane. Early studies in sea urchin eggs and fibroblasts indicated a role for calcium-driven vesicle transport and exocytosis in plasma membrane resealing [22, 41]. Calcium was also shown to trigger the local accumulation and fusion of internal membrane vesicles with the plasma membrane to 'patch' membrane disruption sites [42, 43]. Notably, the reduction of plasma membrane surface tension was found to be required for

calcium-dependent plasma membrane resealing [44]. Our finding that higher shear stress and cell strain correlated with the FM 1-43 fluorescence intensity in a microfluidic assay supports the hypothesis that the protective effect of calcium against shear stress-induced cell damage and death is based on a more efficient plasma membrane resealing.

However, calcium might also affect cellular shear stress vulnerability through its effects on the F-actin cytoskeleton in the cell cortex. Calcium has been shown to directly affect actin-polymerization through proteins such as calcium-calmodulin kinase, L-plastin or villin [45–47], and a calcium-mediated 'actin-reset' mechanism was recently found to mediate the adaptive remodelling of cortical F-actin in response to mechanical perturbation [23]. Whether exocytosis-driven membrane resealing, Ca^{2+}-mediated actin-cortex remodelling, or a combination of both mediate the improved shear stress vulnerability in the presence of calcium, will need to be addressed in further studies. Altogether, we recommend the supplementation of alginate-based and other bioinks with physiological concentrations of calcium to reduce shear stress induced cell damage and improve cell survival. Our findings further raise the question whether bioink supplementation with other physiologically active compounds, such as serum, may also help to modulate the shear stress vulnerability of printed cells.

Data availability statement

The data that support the findings of this study are available upon reasonable request from the authors.

Acknowledgments

This research was funded by the Deutsche Forschungsgemeinschaft (DFG, German Research Foundation)—Project Number 326998133—TRR 225 (subprojects A01, B06, C01, C02).

ORCID iDs

Richard Gerum https://orcid.org/0000-0001-5893-2650
Ben Fabry https://orcid.org/0000-0003-1737-0465
Ingo Thievessen https://orcid.org/0000-0003-3375-1073

References

[1] Mandrycky C, Wang Z, Kim K and Kim D 2017 3D bioprinting for engineering complex tissues Biotechnology Advances **34** 422–34
[2] Roth E A, Xu T, Das M, Gregory C, Hickman J J and Boland T 2004 Inkjet printing for high-throughput cell patterning *Biomaterials* **25** 3707–15
[3] Odde D J and Renn M J 2000 Laser-guided direct writing of living cells *Biotechnol. Bioeng.* **67** 312–8
[4] Pfister A, Landers R, Laib A, Hübner U, Schmelzeisen R and Mülhaupt R 2004 Biofunctional rapid prototyping for tissue-engineering applications: 3D bioplotting versus 3D printing *J. Polym. Sci.* A **42** 624–38
[5] Ozbolat I T and Hospodiuk M 2016 Current advances and future perspectives in extrusion-based bioprinting *Biomaterials* **76** 321–43
[6] Ramesh S, Harrysson O L A, Rao P K, Tamayol A, Cormier D R, Zhang Y and Rivero I V 2021 Extrusion bioprinting : recent progress, challenges, and future opportunities *Bioprinting* **21** e00116
[7] Müller S J, Mirzahossein E, Iftekhar E N, Bächer C, Schrüfer S, Schubert D W, Fabry B and Gekle S 2020 Flow and hydrodynamic shear stress inside a printing needle during biofabrication *PLoS One* **15** 1–15
[8] Augst A D, Kong H J and Mooney D J 2006 Alginate hydrogels as biomaterials *Macromol. Biosci.* **6** 623–33
[9] Fedorovich N E, Alblas J, De Wijn J R, Hennink W E, Verbout A B J and Dhert W J A 2007 Hydrogels as extracellular matrices for skeletal tissue engineering: state-of-the-art and novel application in organ printing *Tissue Eng.* **13** 1905–25
[10] Fedorovich N E, Schuurman W, Wijnberg H M, Prins H J, Van Weeren P R, Malda J, Alblas J and Dhert W J A 2012 Biofabrication of osteochondral tissue equivalents by printing topologically defined, cell-laden hydrogel scaffolds *Tissue Eng.* C **18** 33–44
[11] Burdick J A and Prestwich G D 2011 Hyaluronic acid hydrogels for biomedical applications *Adv. Mater.* **23** H41–H56
[12] Kogan G, Šoltés L, Stern R and Gemeiner P 2007 Hyaluronic acid: a natural biopolymer with a broad range of biomedical and industrial applications *Biotechnol. Lett.* **29** 17–25
[13] Xu X, Jha A K, Harrington D A, Farach-Carson M C and Jia X 2012 Hyaluronic acid-based hydrogels: from a natural polysaccharide to complex networks *Soft Matter* **8** 3280–94
[14] Nair K, Gandhi M, Khalil S, Yan K C, Marcolongo M, Barbee K and Sun W 2009 Characterization of cell viability during bioprinting processes *Biotechnol. J.* **4** 1168–77
[15] Blaeser A, Filipa D, Campos D, Puster U, Richtering W, Stevens M M and Fischer H 2015 Controlling shear stress in 3D bioprinting is a key factor to balance printing resolution and stem cell integrity *Avanced Healthcare Materials* **5** 326–33
[16] Ning L, Yang B, Mohabatpour F, Betancourt N, Sarker M D, Papagerakis P and Chen X 2020 Process-induced cell damage: pneumatic versus screw-driven bioprinting *Biofabrication* **12** 25011
[17] Aguado B A, Mulyasasmita W, Su J, Lampe K J and Heilshorn S C 2012 Improving viability of stem cells during syringe needle flow through the design of hydrogel cell carriers *Tissue Eng.* A **18** 806–15
[18] Guvendiren M, Lu H D and Burdick J A 2012 Shear-thinning hydrogels for biomedical applications *Soft Matter* **8** 260–72
[19] Müller M, Öztürk E, Arlov Ø, Gatenholm P and Zenobi-Wong M 2017 Alginate sulfate–nanocellulose bioinks for cartilage bioprinting applications *Ann. Biomed. Eng.* **45** 210–23
[20] Berridge M J, Lipp P and Bootman M D 2000 The versatility and universality of calcium signalling *Nat. Rev. Mol. Cell Biol.* **1** 11–21
[21] Dolmetsch R E, Xu K and Lewis R S 1998 Calcium oscillations increase the efficiency and specificity of gene expression *Nature* **392** 933–6
[22] Steinhardt R A, Bi G and Alderton J M 1994 Cell membrane resealing by a vesicular mechanism similar to neurotransmitter release *Science* **263** 390–3
[23] Wales P *et al* 2016 Calcium-mediated actin reset (CaAR) mediates acute cell adaptations *Elife* **5** 1–31
[24] Marczenke M, Piccini I, Mengarelli I, Fell J, Röpke A, Seebohm G, Verkerk A O and Greber B 2017 Cardiac subtype-specific modeling of $K_v1.5$ ion channel

deficiency using human pluripotent stem cells *Front. Physiol.* **8** 1–11
[25] Genç H, Hazur J, Karakaya E, Dietel B, Bider F, Groll J, Alexiou C, Boccaccini A R, Detsch R and Cicha I 2021 Differential responses to bioink-induced oxidative stress in endothelial cells and fibroblasts *Int. J. Mol. Sci.* **22** 1–21
[26] Schindelin J *et al* 2012 Fiji—an open platform for biological image analysis *Nat. Methods* **9** 676–82
[27] Gerum R C, Richter S, Fabry B and Zitterbart D P 2017 ClickPoints: an expandable toolbox for scientific image annotation and analysis *Methods Ecol. Evol.* **8** 750–6
[28] Lautscham L A *et al* 2015 Migration in confined 3D environments is determined by a combination of adhesiveness, nuclear volume, contractility, and cell stiffness *Biophys. J.* **109** 900–13
[29] Gerum R *et al* 2022 Viscoelastic properties of suspended cells measured with shear flow deformation cytometry *bioRxiv Preprint* https://doi.org/10.1101/2022.01.11.475843 (posted online 12 January 2022)
[30] Betz W J, Mao F and Smith C B 1996 Imaging exocytosis and endocytosis *Curr. Opin. Neurobiol.* **6** 365–71
[31] Ning L, Guillemot A, Zhao J, Kipouros G and Chen X 2016 Influence of flow behavior of alginate-cell suspensions on cell viability and proliferation *Tissue Eng.* C **22** 75–87
[32] Van Den Bulcke A I, Bogdanov B, De Rooze N, Schacht E H, Cornelissen M and Berghmans H 2000 Structural and rheological properties of methacrylamide modified gelatin hydrogels *Biomacromolecules* **1** 31–38
[33] McDade J R, Naylor M T and Michele D E 2021 Sarcolemma wounding activates dynamin-dependent endocytosis in striated muscle *FEBS J.* **288** 160–74
[34] Bansal D, Miyake K, Vogel S S, Groh S, Chen C C, Williamson R, McNeil P L and Campbell K P 2003 Defective membrane repair in dysferlin-deficient muscular dystrophy *Nature* **423** 168–72
[35] McNeil P L, Miyake K and Vogel S S 2003 The endomembrane requirement for cell surface repair *Proc. Natl Acad. Sci. USA* **100** 4592–7
[36] Li M, Tian X, Kozinski J A, Chen X and Hwang D K 2015 Modeling mechanical cell damage in the bioprinting process employing a conical needle *J. Mech. Med. Biol.* **15** 1–15
[37] Müller S J, Weigl F, Bezold C, Bächer C, Albrecht K and Gekle S 2021 A hyperelastic model for simulating cells in flow *Biomech. Model. Mechanobiol.* **20** 509–20
[38] Lin R C and Scheller R H 2000 Mechanisms of synaptic vesicle exocytosis *Annu. Rev. Cell Dev. Biol.* **16** 19–49
[39] Ahluwalia J P, Topp J D, Weirather K, Zimmerman M and Stamnes M 2001 A role for calcium in stabilizing transport vesicle coats *J. Biol. Chem.* **276** 34148–55
[40] Shao X, Li Q, Mogilner A, Bershadsky A D and Shivashankar G V 2015 Mechanical stimulation induces formin-dependent assembly of a perinuclear actin rim *Proc. Natl Acad. Sci. USA* **112** E2595–601
[41] Bi G Q, Alderton J M and Steinhardt R A 1995 Calcium-regulated exocytosis is required for cell membrane resealing *J. Cell Biol.* **131** 1747–58
[42] Miyake K and McNeil P L 1995 Vesicle accumulation and exocytosis at sites of plasma membrane disruption *J. Cell Biol.* **131** 1737–45
[43] Terasaki M, Miyake K and McNeil P L 1997 Large plasma membrane disruptions are rapidly resealed by Ca^{2+}-dependent vesicle-vesicle fusion events *J. Cell Biol.* **139** 63–74
[44] Togo T, Alderton J M, Bi G Q and Steinhardt R A 1999 The mechanism of facilitated cell membrane resealing *J. Cell Sci.* **112** 719–31
[45] Wang Q, Chen M, Schafer N P, Bueno C, Song S S, Hudmon A, Wolynes P G, Neal Waxham M and Cheung M S 2019 Assemblies of calcium/calmodulin-dependent kinase II with actin and their dynamic regulation by calmodulin in dendritic spines *Proc. Natl Acad. Sci. USA* **116** 18937–42
[46] Ishida H, Jensen K V, Woodman A G, Hyndman M E and Vogel H J 2017 The calcium-dependent switch helix of L-plastin regulates actin bundling *Sci. Rep.* **7** 1–12
[47] Walsh T P, Weber A, Davis K, Bonder E and Mooseker M 1984 Calcium dependence of villin-induced actin depolymerization *Biochemistry* **23** 6099–102